Reports

Crystal Structure of $Tl_2Ba_2Ca_2Cu_3O_{10}$, a 125 K Superconductor

C. C. Torardi, M. A. Subramanian, J. C. Calabrese,
J. Gopalakrishnan, K. J. Morrissey, T. R. Askew, R. B. Flippen,
U. Chowdhry, A. W. Sleight

There is now a new series of high-temperature superconductors that may be represented as $(A^{III}O)_2A_2^{II}Ca_{n-1}Cu_nO_{2+2n}$ where A^{III} is Bi or Tl, A^{II} is Ba or Sr, and n is the number of Cu-O sheets stacked consecutively. There is a general trend toward higher transition temperatures as n increases. The highest n value for a bulk phase is three and is found when A^{III} is Tl. This compound, $Tl_2Ba_2Ca_2Cu_3O_{10}$, has the highest transition temperature (~125 K) of any presently known bulk superconductor. The structure of $Tl_2Ba_2Ca_2Cu_3O_{10}$ has been determined from single-crystal x-ray diffraction data and is tetragonal, with $a = 3.85$ Å and $c = 35.9$ Å. No superstructure is observed, and the material is essentially twin-free. Electron microscopy in the Tl/Ba/Ca/Cu/O system has revealed intergrowths where $n = 5$; such regions may well be responsible for the superconducting onset behavior observed in this system at about 140 K.

Michel *et al.* reported (*1*) superconductivity at about 20 K in the Bi/Sr/Cu/O system for a compound that we now know (*2*) to be $Bi_2Sr_2CuO_6$. Maeda *et al.* reported (*3*) superconductivity at temperatures somewhat higher than 100 K in the Bi/Sr/Ca/Cu/O system. This was rapidly confirmed (*4*), and some phase identification studies in this system were presented (*5*). We determined the structure (*6*) of a high transition temperature (T_c) superconductor with the ideal composition $Bi_2Sr_2CaCu_2O_8$, and this was quickly confirmed independently by others (*7, 8*). More recently, Sheng and Hermann reported (*9*) high-temperature superconductivity in the Tl/Ba/Ca/Cu/O system. Hazen *et al.* (*10*) identified two phases in this system as $Tl_2Ba_2CaCu_2O_8$ and $Tl_2Ba_2Ca_2Cu_3O_{10}$. We have reported (*2, 11*) on the structure of $Tl_2Ba_2CaCu_2O_8$ as well as $Tl_2Ba_2CuO_6$. We now report on the synthesis of single-phase $Tl_2Ba_2Ca_2Cu_3O_{10}$. Crystals were also grown of this phase, and the structure has been determined from single-crystal x-ray diffraction data.

Various samples in the Tl/Ba/Ca/Cu/O system were prepared by thoroughly mixing Tl_2O_3, CaO_2, BaO_2, and CuO in various ratios. The mixtures were pressed into pellets, sealed in gold tubes (1.3 cm in diameter and 10 cm in length), and heated at 850° to 925°C for varying times. Under our preparatory conditions, essentially single-phase $Tl_2Ba_2Ca_2Cu_3O_{10}$ was made by heating the mixture containing stoichiometric quantities to 890°C for 1 hour. A powder x-ray diffraction pattern showed a strong peak with a *d*-spacing close to 18 Å, and all the peaks could be indexed on the basis of a tetragonal cell with $a \sim 3.85$ and $c \sim 35.9$ Å. Absence of peaks with a *d*-spacing closer to ~14.7 Å indicated that little or no $Tl_2Ba_2CaCu_2O_8$ is present. However, when the same starting mixtures were heated to 890°C for longer durations (>2 hours) or at temperatures >900°C for shorter times, $Tl_2Ba_2CaCu_2O_8$ occurred as a major phase and $Tl_2Ba_2Ca_2Cu_3O_{10}$ as a minor phase. Figure 1 shows a comparison of the powder x-ray diffraction patterns for $Tl_2Ba_2Ca_{n-1}Cu_nO_{4+2n}$ for $n = 1, 2$, and 3. The characteristic peak at low angles shifts to higher *d* values (lower 2θ) as n increases because the *c* axis increases with the number of Cu-O layers. We have not seen x-ray diffraction evidence for bulk phases where n is greater than three.

Single crystals of $Tl_2Ba_2Ca_2Cu_3O_{10}$ were grown from starting compositions containing excess Ca and Cu (2Tl:2Ba:3Ca:4Cu) in sealed gold tubes. Reaction mixtures were heated to 920°C for 3 hours and cooled to 300°C at a rate of 5°C per minute. Attempts to grow $Tl_2Ba_2Ca_2Cu_3O_{10}$ crystals from compositions with excess Cu alone (2:2:2:4) always resulted in the formation of 2:2:1:2 crystals and calcium-copper oxides.

Flux exclusion measurements showed that the superconducting transitions varied widely (127 to 116 K) depending on the synthesis conditions. Four-probe resistivity measurements on a typical sample showed apparent zero resistivity (10^{-8} ohms) at 122 K (Fig. 2). Flux exclusion measurements on the same sample showed an abrupt transition around 125 K. Similar results have been obtained by others (*12*).

Electron microscopy studies were carried out by using both a Philips CM12 and a JEOL 2000EX. Electron diffraction showed $Tl_2Ba_2Ca_2Cu_3O_{10}$ to be tetragonal with $a = 3.86$ Å and $c = 35.95$ Å. Lattice imaging clearly showed the Tl-O double layers and the Cu-O triple layers. However, a prominent defect in some of the particles was the presence of five consecutive Cu-O layers. Figure 3 is an electron diffraction pattern showing reflections from the regions of intergrowth. A spacing of 48 Å was measured for *c* in extended regions of this intergrowth. Although some other defects are also observed, $Tl_2Ba_2Ca_2Cu_3O_{10}$ is essentially twin-free as expected from its tetragonal symmetry. The morphology of $Tl_2Ba_2Ca_2Cu_3O_{10}$ was, like the other Tl/Ba phases, platy, but not micaceous.

Single-crystal x-ray diffraction information for $Tl_2Ba_2Ca_2Cu_3O_{10}$ is summarized in Table 1. Initially, several black, plate-shaped crystals were examined on the x-ray diffractometer. Scans along the [001] direction for many of these crystals showed incommensurate diffraction peaks whose 2θ positions

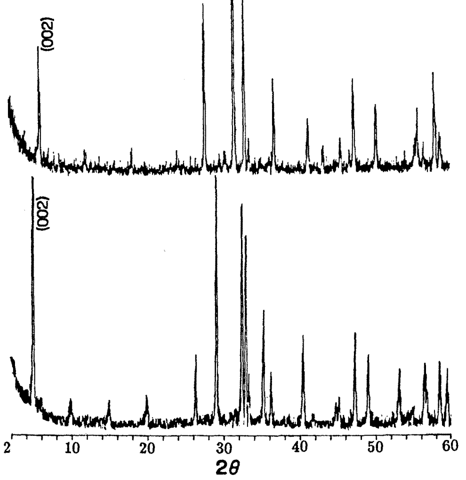

Fig. 1. Powder x-ray diffraction intensity data with CuKα radiation for the $Tl_2Ba_2Ca_{n-1}Cu_nO_{4+2n}$ series for (**top**) $n = 1$, (**center**) $n = 2$, and (**bottom**) $n = 3$.

Central Research and Development Department, E. I. du Pont de Nemours and Company, Experimental Station, Wilmington, DE 19898.

varied from one crystal to another. This is consistent with the formation of layered intergrowths composed of a varying number of Cu-O sheets (for example, $n = 1, 2, 3$, or more in $Tl_2Ba_2\text{-}Ca_{n-1}Cu_nO_{4+2n}$) alternating with double Tl-O sheets stacked along the z direction. A crystal that showed no extra peaks along [001] was selected for data collection. It was indexed as tetragonal with cell constants of $a = 3.85$ and $c = 35.88$ Å. As observed (*2, 11*) in the other Tl-Ba compounds with $n = 1$ and 2, no satellite peaks, similar to those found in $Bi_2Sr_2CaCu_2O_8$, were seen in the [100], [010], or [110] directions. The data were reduced to structure factors, corrected for absorption, and averaged in I4/mmm symmetry. Atomic positions were calculated by using the structure of $Tl_2Ba_2\text{-}CaCu_2O_8$ (*11*) as a model and making allowance for two additional Cu-O and two Ca sheets in the unit cell. The structure was refined by full-matrix least-squares analysis in which we used neutral atom scattering factor curves with anomalous scattering terms for the metal atoms, and anisotropic thermal motion for all but one of the O atoms. Occupation factors for the metal atoms were refined and found to be low for Tl and high for Ca, indicating substitution of Tl on the Ca site as seen in $Tl_2Ba_2CaCu_2O_8$ (*11*). The level of substitution was approximated by refining the site multipliers as a function of the ratio of the Tl and Ca scattering factor curves, assuming that all metal atom sites are occupied. This gave a 15% occupancy of Ca on the Tl site, and a 12% occupancy of Tl on the Ca site. However, it is difficult to conclude whether or not the thallium sheets are fully occupied. The refinement indicated large thermal motion, $B = 2.8 \pm 0.10$ Å^2, for the oxygen atom [O(4)] located in the plane of the Tl sheets as previously seen in the structures (*2, 11*) of $Tl_2Ba_2CuO_6$ and $Tl_2Ba_2CaCu_2O_8$. Refining this O atom off of its ideal 1/2, 1/2, z (4mm) site results in a 0.4 Å displacement and creates a locally distorted Tl environment (discussed below), but the isotropic thermal parameter refines to a small negative value, -0.4 ± 0.7 (Table 2). The largest peak in a final difference Fourier map was 0.25 e/Å^3 located 1.1 Å from O(1). Positional and thermal parameters for $Tl_2Ba_2Ca_2Cu_3O_{10}$ are given in Tables 2 and 3. Interatomic distances and angles are listed in Table 4.

The crystal structures of the $Tl_2Ba_2\text{-}Ca_{n-1}Cu_nO_{4+2n}$ series are shown in Fig. 4. The structures differ from one another by the number of consecutive Cu-O sheets. In $Tl_2Ba_2Ca_2Cu_3O_{10}$, triple sheets of corner-sharing square-planar CuO_4 groups are oriented parallel to the (001) plane. Additional oxygen atoms are located above and below the triple Cu-O sheets and are positioned at a distance of 2.5 Å from the copper atoms. There are no oxygen atoms between the triple Cu-O sheets analogous to the double sheets of the $n = 2$ thallium and bismuth compounds. The Cu-O bond distances in the middle sheet are 1.925 Å whereas those in the two outer sheets are slightly longer, 1.927 Å. The individual Cu-O sheets are separated by 3.2 Å (Cu-Cu distance) with calcium (and some thallium) ions coordinated to eight O atoms with C_{4v} site symmetry

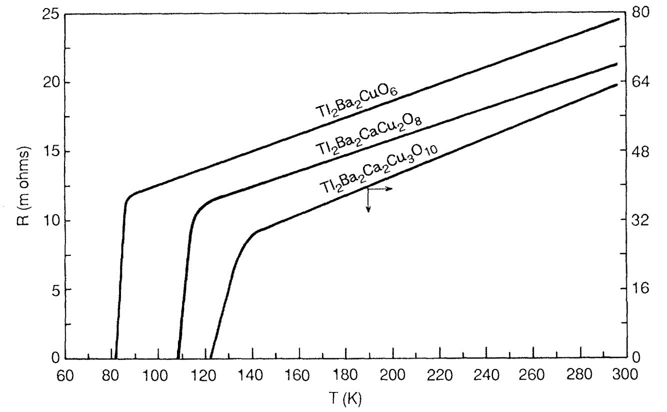

Fig. 2. Electrical resistance versus temperature for the $Tl_2Ba_2Ca_{n-1}Cu_nO_{4+2n}$ series.

Table 1. Summary of crystallographic information for $Tl_2Ba_2Ca_2Cu_3O_{10}$

Dimensions (mm)	0.08 × 0.09 × 0.01
Diffractometer	Enraf-Nonius CAD4
Radiation	Mo Kα
Monochromator	Graphite
Formula weight	1114.2
Crystal system	Tetragonal
Space group	I4/mmm (no. 139)
Cell constants (Å)	$a = 3.8503 \pm 0.0006$
	$c = 35.88 \pm 0.03$
Temperature	Ambient
Calc. density (g · cm^{-3})	6.96 ($Z = 2$)
Scan mode	ω
2θ range (°)	0 to 60
Octants	+ + +, − + +
μ (cm^{-1})	446.7
Absorption correction	Analytical
Transmission factors	0.055 to 0.502
Total reflections	1807
Independent reflections	215 ($I > 3\sigma$)
Data/parameters	7.2
R	0.069
R_w	0.074

Table 2. Position* and thermal† parameters for the atoms of $Tl_2Ba_2Ca_2Cu_3O_{10}$.

Atom	Site	x	y	z§	B (Å^2)§
Tl(1)	4e	0.50	0.50	0.2201(1)	2.1(1)
Ba(1)	4e	0.00	0.00	0.1448(1)	0.6(1)
Cu(1)	2b	0.50	0.50	0.00	0.3(1)
Cu(2)	4e	0.50	0.50	0.0896(2)	0.7(1)
Ca(1)	2a	0.00	0.00	0.0463(2)	1.2(1)
O(1)	4c	0.50	0.00	0.00	0.9(9)
O(2)	8g	0.50	0.00	0.0875(6)	1.2(6)
O(3)	4e	0.50	0.50	0.1588(13)	2.3(9)
O(4)‡	4e	0.50	0.50	0.2719(14)	2.08(10)

*Space group I4/mmm (no. 139). †All atoms except O(4) refined with anisotropic thermal parameters—equivalent isotropic thermal parameter is listed. ‡Refining this atom off of the 4e site and statistically distributed on the 16n sites gives $x = 0.60 \pm 0.01$, $y = 0.50$, $z = 0.2724 \pm 0.0009$, and $B = -0.4 \pm 0.7$. §Numbers in parentheses are uncertainties in last decimal place.

Table 3. Anisotropic thermal parameters* (Å^2) for the atoms of $Tl_2Ba_2Ca_2Cu_3O_{10}$.

Atom	B_{11}†	B_{22}†	B_{33}†
Tl(1)	2.7(1)	2.7	1.0(1)
Ba(1)	0.4(1)	0.4	1.0(1)
Cu(1)	0.2(2)	0.2	0.4(2)
Cu(2)	0.2(2)	0.2	1.6(2)
Ca(1)	0.8(3)	0.8	2.2(3)
O(1)	1.3(18)	0.7(16)	0.8(9)
O(2)	1.1(13)	0.6(12)	1.8(8)
O(3)	0.9(14)	0.9	5.1(24)

*These are the constants in the expression $\exp[-0.25(B_{11}h^2a^{*2} \ldots + 2(B_{12}hka^*b^* \ldots))]$; $B_{12} = B_{13} = B_{23} = 0.0$. †Numbers in parentheses are uncertainties in last decimal place.

Table 4. Interatomic distances and angles in $Tl_2Ba_2Ca_2Cu_3O_{10}$.

Distances (Å)		
Cu(1)-O(1)	1.9252(3)	(×4)
Cu(2)-O(2)	1.927(1)	(×4)
Cu(2)-O(3)	2.48(5)	(×1)
Cu(1)-Cu(2)	3.214(6)	(intersheet)
Tl(1)-O(3)	2.20(5)	(×1)
Tl(1)-O(4)*	1.92(3)	(×1)
Tl(1)-O(4)*	2.48(3)	(×2)
Tl(1)-O(4)*	3.02(4)	(×2)
Ba(1)-O(2)	2.82(2)	(×4)
Ba(1)-O(3)	2.768(9)	(×4)
Ba(1)-O(4)*	2.99(3)	(×1)
Ca(1)-O(1)	2.542(5)	(×4)
Ca(1)-O(2)	2.427(14)	(×4)
Angles (degrees)		
O(1)-Cu(1)-O(1)	180.0	(×2)
O(1)-Cu(1)-O(1)	90.0	(×4)
Cu(1)-O(1)-Cu(1)	180.0	(×1)
O(2)-Cu(2)-O(2)	175(1)	(×2)
O(2)-Cu(2)-O(2)	89.91(6)	(×4)
O(2)-Cu(2)-O(3)	92.3(7)	(×4)
Cu(2)-O(2)-Cu(2)	175(1)	(×1)

*O(4) on the 16n sites of space group I4/mmm (no. 139).

and an average Ca-O distance of 2.48 Å.

Barium ions reside just above and below the Cu-O triple sheets in nine-coordination with oxygen. The Ba-Cu-Ca-Cu-Ca-Cu-Ba slabs in $Tl_2Ba_2Ca_2Cu_3O_{10}$ alternate with a double thallium-oxygen layer giving a layer repeat sequence of ···Tl-Tl-Ba-Cu-Ca-Cu-Ca-Cu-Ba··· along the *z* direction. Thallium bonds to six oxygen atoms in a distorted octahedral arrangement where the octahedra share edges within the *ab* plane. A subtle disorder is suggested by the relatively larger basal ($B_{11} = B_{22}$) thermal parameters for Tl (Table 3) and the large thermal parameter for the intrasheet O atom, O(4). This is evidence for the existence of a locally distorted thallium environment where the Tl and O atoms within the sheets are statistically positioned around the 4*e* sites in order to form shorter Tl-O bonds. The average Tl-O bond distance within the sheet, with Tl and O(4) on the 4*e* sites, is 2.72 Å and is significantly longer than the sum of ionic radii, 2.28 Å, suggesting that Tl and O actually reside off of this special position. With O(4) shifted to the 16*n* sites, two short and two long Tl-O bonds are formed, 2.48 and 3.02 Å. This is identical to the situation seen in the thallium-oxygen sheets of the $Tl_2Ba_2CuO_6$ and $Tl_2Ba_2CaCu_2O_8$ compounds (*2, 11*).

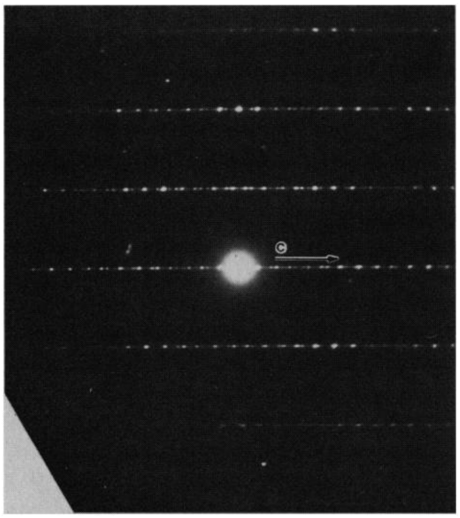

Fig. 3. Electron diffraction pattern recorded with [001] nearly parallel to the electron beam.

For the $(A^{III}O)_2A_2^{II}Ca_{n-1}Cu_nO_{2+2n}$ series of compounds, we have now clearly established that *n* may reach three as a bulk phase. There is a general trend of increasing T_c with increasing *n* that, if linear, would suggest that room temperature superconductivity might be achieved if *n* reached ten. Although bulk materials have not yet been prepared for Tl phases with *n* greater than three or for Bi phases with *n* greater than two, we find intergrowths with *n* up to five in both systems. It is thus tempting to conclude that the onset behavior at about 120 K in the $Bi_2Sr_2Ca_{n-1}Cu_nO_{4+2n}$ system and at about 140 K in the $Tl_2Ba_2Ca_{n-1}Cu_nO_{4+2n}$ system is due to these intergrowths where *n* values of five are achieved. A major challenge is now to prepare bulk phases where *n* is five or greater.

One apparent trend with increasing *n* for $Tl_2Ba_2Ca_{n-1}Cu_nO_{4+2n}$ phases is that the Cu-O distance in the sheets decreases as the *a* axis decreases: 1.933 Å for $n = 1$, 1.928 Å for $n = 2$ and 1.926 Å for $n = 3$. This suggests a relationship between Cu-O distance and T_c as has been found for $La_{2-x}A_xCuO_4$ phases (*13*). However, the corresponding distances in the $Bi_2Sr_2Ca_{n-1}Cu_nO_{4+2n}$ are shorter (~1.90 Å), yet T_c's are generally lower. Thus, if the Cu-O distance influences T_c, there are other competing factors.

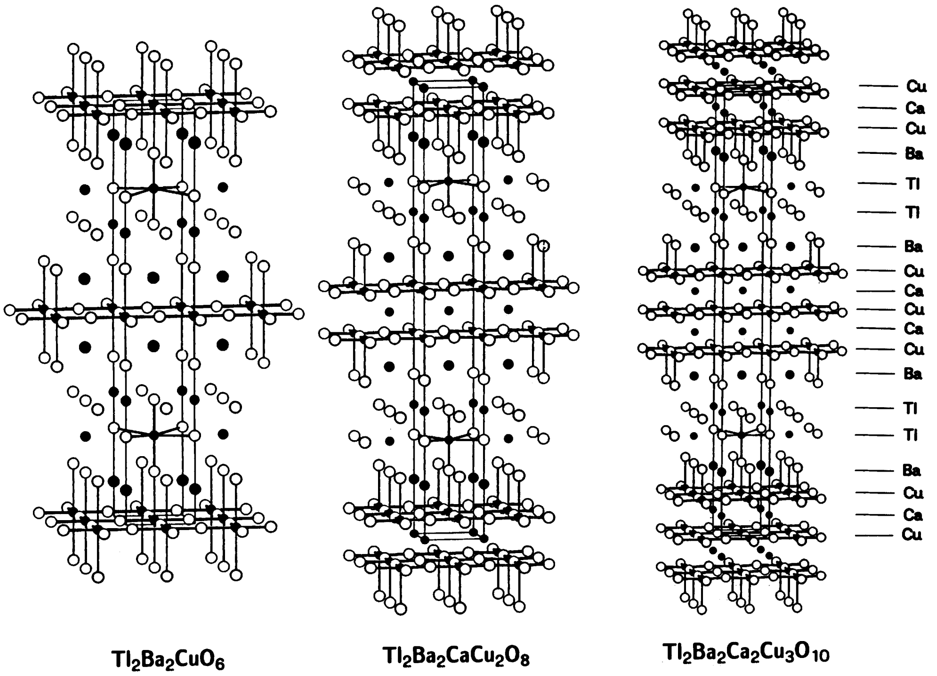

Fig. 4. A comparison of the structures of $Tl_2Ba_2Ca_{n-1}Cu_nO_{4+2n}$ for $n = 1$, 2, and 3. Metal atoms are shaded and Cu-O bonds are shown.

The Cu-O sheets in the $Tl_2Ba_2Ca_{n-1}Cu_nO_{4+2n}$ phase are somewhat flatter than the sheets in the analogous Bi phases. This is at least in part related to the somewhat longer Cu-O distances in the Tl phases. The Cu-O sheets are buckled in both $Bi_2Sr_2CuO_6$ (*2*) and $Bi_2Sr_2CaCu_2O_8$ (*6*); however, this sheet is flat in $Tl_2Ba_2CuO_6$ (*2*) and the Cu-O sheets of $Tl_2Ba_2CaCu_2O_8$ are just slightly buckled. In $Tl_2Ba_2Ca_2Cu_3O_{10}$, the middle sheet is constrained by symmetry to be flat. Flat sheets presumably stack better than buckled sheets, and this could then be the reason that $n = 3$ is easier to achieve in the Tl system. Flatness of Cu-O sheets is directly related to the Cu-O-Cu bond angle in the Cu-O sheets, and it is possible that phonons connected to bending this bond are related to superconductivity through an electron-phonon coupling mechanism.

Another factor that could be influencing T_c is the average oxidation state of Cu. As written, $(A^{III}O)_2A_2^{II}Ca_{n-1}Cu_nO_{2+2n}$ phases would be expected to contain copper only as Cu^{II}. However, it is likely that Cu^{III} is always present in these materials owing to excess oxygen (for example, $Bi_2Sr_2CaCu_2O_{8+y}$), a cation deficiency ($Tl_{2-x}Ba_2CaCu_2O_8$), or redox chemistry owing to band overlap ($Tl^{III}_{2-x}Tl^{II}_xBa_2CaCu^{II}_{2-x}Cu^{III}_xO_8$). In the last case, Tl^{II} merely indicates 6*s* electrons delocalized in a 6*s* band such that the Tl-O double layer would be metallic.

Note added in proof: The metal atom positions for the thallium superconductors described in (*14*) were approximately correct. However, the oxygen positions were largely wrong, resulting in incorrect coordinations for both copper and thallium.

REFERENCES AND NOTES

1. C. Michel *et al.*, *Z. Phys. B* **68**, 421 (1987).
2. C. C. Torardi *et al.*, *Phys. Rev. B*, in press.
3. H. Maeda, Y. Tanaka, M. Fukutomi, T. Asano, *Jpn. J. Appl. Phys.* **27**, L209 (1988).
4. C. W. Chu *et al.*, *Phys. Rev. Lett.* **60**, 941 (1988).
5. R. M. Hazen *et al.*, *ibid.*, p. 1174.
6. M. A. Subramanian *et al.*, *Science* **239**, 1015 (1988).
7. J. M. Tarascon *et al.*, *Phys. Rev. B.*, in press.
8. S. A. Sunshine *et al.*, *Phys. Rev. Lett.*, in press.
9. Z. Z. Sheng and A. M. Hermann, *Nature* **332**, 55 (1988); *ibid.*, p. 138.
10. R. M. Hazen *et al.*, *Phys. Rev. Lett.* **60**, 1657 (1988).
11. M. A. Subramanian *et al.*, *Nature* **332**, 420 (1988).
12. S. S. P. Parkin *et al.*, *Phys. Rev. Lett.*, in press.
13. K. Fueki *et al.*, in *Chemistry of High Temperature Superconductors*, D. L. Nelson, J. S. Whittingham, T. F. George, Eds. (American Chemical Society, Washington, DC, 1987), p. 38.

14. R. Pool, *Science* **240**, 147 (1988).
15. We thank the following Du Pont colleagues for their assistance with this publication: P. M. Kelly, C. R. Walther, R. A. Oswald, W. J. Marshall, L. F. Lardear, D. L. Smith, D. M. Groski, L. Cooke, C. M. Foris, A. J. Pawlowski, G. M. Hyatt, M. W. Sweeten, and N. Budynkiewicz.

30 March 1988; accepted 1 April 1988

Stratospheric Response to Trace Gas Perturbations: Changes in Ozone and Temperature Distributions

GUY BRASSEUR AND MATTHEW H. HITCHMAN

The stratospheric concentration of trace gases released in the atmosphere as a result of human activities is increasing at a rate of 5 to 8 percent per year in the case of the chlorofluorocarbons (CFCs), 1 percent per year in the case of methane (CH_4), and 0.25 percent per year in the case of nitrous oxide (N_2O). The amount of carbon dioxide (CO_2) is expected to double before the end of the 21st century. Even if the production of the CFCs remains limited according to the protocol for the protection of the ozone layer signed in September 1987 in Montreal, the abundance of active chlorine (2 parts per billion by volume in the early 1980s) is expected to reach 6 to 7 parts per billion by volume by 2050. The impact of these increases on stratospheric temperature and ozone was investigated with a two-dimensional numerical model. The model includes interactive radiation, wave and mean flow dynamics, and 40 trace species. An increase in CFCs caused ozone depletion in the model, with the largest losses near the stratopause and, in the vertical mean, at high latitudes. Increased CO_2 caused ozone amounts to increase through cooling, with the largest increases again near 45 kilometers and at high latitudes. This CO_2-induced poleward increase reduced the CFC-induced poleward decrease. Poleward and downward ozone transport played a major role in determining the latitudinal variation in column ozone changes.

HUMAN ACTIVITY HAS CAUSED A marked increase in the concentration of certain important trace gases in the atmosphere. These gases can have a significant impact on ozone, either directly through photochemistry or indirectly by changing the radiative budget and hence the temperature and chemistry (*1*). If the temperature structure changes, transport of chemicals by the mean circulation and waves can change. Ozone absorbs ultraviolet (UV) insolation, accounting for the basic structure of the stratosphere, in which temperature increases with altitude from the tropopause near 15 km to the stratopause near 50 km, and shields the biosphere from potentially harmful effects. It is of considerable interest to estimate the distribution in latitude and altitude of ozone and temperature changes due to increased trace gases.

Two-dimensional models (2-D; latitude and altitude) represent transport in a more realistic way than 1-D models, which provide globally averaged vertical distributions (*2*). Most of the previous perturbation studies performed with 2-D models indicated that the expected ozone depletion due to chlorofluorocarbons (CFCs) should be two to three times larger in the polar regions than in the tropics, with the strongest latitudinal gradient in depletion occuring in spring (*3, 4*). Other studies (*5, 6*) showed that increases in CO_2 can enhance ozone amounts, with the largest increases near the pole. The recent study (*6*) raised the possibility that CFC-induced reductions might be reversed by larger CO_2-induced increases at high latitudes. The magnitude and sign of changes in the ozone column (number of ozone molecules above an area at the earth's surface) is governed primarily by changes in the lower stratosphere where most of the ozone resides. In this altitude range, chemistry, dynamics, and radiation play equally important roles, so that these processes and their interactions need to be represented as accurately as possible. The purpose of the present study is to assess, as a function of latitude and altitude, the response of the middle atmosphere to specified anthropogenic perturbations.

Ozone (O_3) is destroyed by chemical recombination with atomic oxygen, a process that is catalyzed by the presence of radicals such as OH, NO, ClO, and BrO (*1*). When CFCs reach the stratosphere they can be photodissociated, with the added chlorine catalytically destroying ozone. The temperature dependence of reactions involving ozone is such that ozone amounts will increase if temperatures decrease. Ozone and temperature are observed to be negatively correlated in the upper stratosphere (*7*). CO_2 efficiently emits infrared radiation to the earth and to space. In the middle atmosphere (tropopause to mesopause, ~80 km), CO_2 increases would lead to more radiation to space and decreased temperatures. Thus CO_2 increases should lead to ozone increases. The latitudinal variation in predicted ozone changes has both photochemical and dynamical contributions. In the sunlight above 25 km, photochemistry plays a major role, whereas below 25 km and in the polar night, dynamical transport is relatively more important (*4*).

The 2-D model used in the present study extends from pole to pole with a latitudinal resolution of 5° and from the surface to 85 km with a vertical resolution of 1 km. The transformed Eulerian mean equations are used (*8*). This allows for a straightforward interpretation of the influence of waves. Absorption of gravity waves (*9*) and Rossby waves (*10*) drives the meridional circulation and mixes constituents in altitude and latitude, respectively. Calculated wave driving and eddy mixing coefficients vary with the evolving model zonal mean wind distribution. Wave driving, mixing coefficients, and temperature are specified below 15 km. Above 15 km, temperature evolves along with changes in the wave-driven circulation and changes in diabatic heating and is calculated with the evolving model fields of ozone and water vapor. The detailed radiative code is similar to the algorithm used in the latest version of the NCAR Community Climate Model (*11*). Included in the radiative calculation are absorption of UV insolation by O_3 and H_2O, near-infrared insolation by O_2 and H_2O, and absorption and emission of infrared radiation by CO_2, O_3, and H_2O. The distributions of chemical species are obtained by integrating their continuity equations, which are expressed in terms of the transformed Eulerian circulation. To avoid numerical problems associated with the broad spectrum of chemical lifetimes involved, the shortest lived species are grouped into quasi-conservative families (*12*). The adopted reaction rate constants, solar irradiance, and absorption cross sections were taken from recent compilations (*13*).

Figure 1 shows the changes in temperature and ozone as a function of latitude and height resulting from (i) a doubling of the CO_2 abundance from the current 350 parts per million by volume (ppmv) (run 1); (ii) increasing the mixing ratio of odd chlorine (Cl_x) in the upper stratosphere from 2.0 to 6.6 parts per billion by volume (ppbv) (run 2); and (iii) a combined scenario (run 3). The model does not include detailed physical parameterizations in the troposphere.

G. Brasseur, Belgian Institute for Space Aeronomy, 1180 Brussels, Belgium.
M. H. Hitchman, National Center for Atmospheric Research, Boulder, CO 80307.